IEEE Access
Multidisciplinary | Rapid Review | Open Access Journal

Received March 25, 2021, accepted April 10, 2021, date of publication April 16, 2021, date of current version May 4, 2021.

Digital Object Identifier 10.1109/ACCESS.2021.3073743

Design Consideration of Fractional Slot Concentrated Winding Interior Permanent Magnet Synchronous Motor for EV and HEV Applications

CHENXI ZHOU[1], XIAOYAN HUANG[1], (Member, IEEE), ZHAOKAI LI[1], AND WENPING CAO[2], (Senior Member, IEEE)

[1]College of Electrical Engineering, Zhejiang University, Hangzhou 310027, China
[2]School of Engineering and Applied Science, Aston University, Birmingham B4 7ET, U.K.

Corresponding author: Zhaokai Li (lzk_zju@zju.edu.cn)

This work was supported in part by the Key Research and Development Program of Zhejiang under Grant 2019C01075, and in part by the Ningbo Science and Technology Innovation 2025 Major Project under Grant 2018B10001 and Grant 2018B10002.

ABSTRACT This paper presents a comprehensive study on the fractional slot concentrated winding (FSCW) interior permanent magnet synchronous motors (IPMSMs) with different pole slot combination for the application of electric vehicle (EV) and hybrid electric vehicle (HEV). Three motors with the same dimension constraint and rated parameters are designed and optimized. With the optimized motors, winding factors and magnetomotive force (MMF), inductances, torque capacity, constant power speed range (CPSR), the losses, the efficiency, demagnetization capability and vibration are investigated and compared. The comparison results show that 12/8 motor and 12/10 motor have their respective unique advantages while 12/14 motor is not as good as the others.

INDEX TERMS Pole slot combination, comparison results, motor performances.

I. INTRODUCTION

Electrical vehicles (EVs) and hybrid electric vehicles (HEVs) have developed rapidly in recent years owing to the increasing focus on the renewable energy. For EVs, permanent magnet synchronous motors (PMSMs) are widely used for its high-power density and high efficiency, compared to other motor candidates, such as induction motor and switching reluctance motor [1]–[3].

In general, PMSMs are equipped with integer slot distributed winding (ISDW), integer slot concentrated winding (ISCW), fractional slot distributed winding (FSDW) or fractional slot concentrated winding (FSCW). Most commercial motors for EVs application are ISDW PMSM, such as 48-slot-8-pole motor or 72-slot-12-pole motor. Nevertheless, PMSMs with FSCW is also a comparative candidate for its short end winding and good flux weakening capability [4], [5].

The associate editor coordinating the review of this manuscript and approving it for publication was Mahdi Pourakbari Kasmaei.

The comparison of ISDW motors and FSCW motors received intensive attention in the past decade. Yang *et al.* compared the 48-slot-8-pole and 12-slot-8-pole interior PMSMs for EV application in terms of torque, efficiency and vibration [1]. The 12-slot-8-pole motor has higher efficiency at low speed but lower efficiency with speed rising for the significant increase of the PM eddy current loss. Besides, the 12-slot-8-pole IPMSM has better performances in cogging effect and pulsating torque, compared to 48-slot-8-pole IPMSM [6]. The constant power speed range (CPSR) of FSCW PMSM is wider [7]. The merit of the lower copper loss for FSCW motors are addressed in [8]. It can be concluded that there is a necessity and feasibility to focus on the study of FSCW motors applied in EV and HEV.

There are a family of pole slot combination for PMSMs to be investigated. Reddy *et al.* highlighted the tradeoffs between 12-slot-10-pole interior and surface PM motors for HEV [9]. The interior PMSM (IPMSM) is chosen in advantage of the reluctance torque and the manufacture simplicity of the motor. In [10], 12-slot-8-pole motor and

12-slot-10-pole IPMSMs are compared for ship application in terms of torque characteristics and radial forces. Inductances from the perspective of the influence by physical dimensions and slot pole combinations are theoretically analyzed and validated with finite-element analysis and experiments [11]. Six machines with different pole slot combinations are chosen and compared in terms of the voltage distortion at various current advancing angle [12]. Terminal voltage distortion largely deteriorated the torque speed characteristics. Prototypes of 12-slot-8-pole and 12-slot-10-pole motors are built and tested to validate the analysis. Similar works are carried out in [13] [14]. The comparative study of the flux weakening capability for a large number of slots per pole per phase (Spp) family is presented in [15]. In [16] and [17], the torque density of the motors is presented. Fornasiero *et al.* introduced a thorough method to select the fractional slot nonoverlapping windings considering torque density, torque ripple, induced rotor losses, and fault-tolerance features [18]. Carraro *et al.* researched on the spoke type motor with different slot pole combination and found that the 18-slot-14-pole motor shows both high torque density and small vibration [19].

In the EV and HEV applications, the FSCW IPMSM has the merit in term of reluctance torque as in the ISDW IPMSM. Despite the reluctance torque might be mitigated due to the FSCW structure, the comprehensive comparison of the FSCW IPMSM performances with different pole slot combinations need to be thoroughly investigated to evaluate the feasibility of FSCW IPMSM for EV and HEV applications.

In this paper, three IPMSMs, including 12-slot-8-pole (12/8) motor, 12-slot-10-pole (12/10) motor and 12-slot-14-pole (12/14) motor are designed and compared. They are designed and optimized in Section II. High torque density, high efficiency, CPSR and demagnetization capability are main consideration for EV and HEV motors, which are simulated and compared in Section III. Noise vibration and harshness (NVH) for the motors are also simulated and analyzed in Section IV. Conclusions are given in Section V.

II. MOTOR DESIGN AND OPTIMIZATION

For EV and HEV applications, the maximum rotation speed of the motor usually exceeds 12000 rpm meanwhile the switching frequency of the commercial inverter is limited within 10 kHz due to the limited install space and high reliability requirement. This leads to the limited selection of the pole pair number for motor, that is, no more than 7. Besides, high pole pair number of motors are preferred in EV for short end winding, which mean the pole pair number is usually no less than 4. As a result, only a small family of pole slot combination can be chosen: 12-slot motor family, (including12 slot-8-pole, 12-slot-10-pole, and 12-slot-14-pole) and 18-slot motor family, including (18-slot-12-pole and 18-slot-14-pole). Odd-slot motor is not considered for the unilateral magnetic force.

For FSCW motors, the harmonic components, the torque performances, the losses and the efficiency have its regularity for a certain slot family. 12-slot motor family are chosen to be analyzed and compared. They are equipped with double layer windings and V-type interior permanent magnet. The control strategy applied for the motors is the maximum torque per ampere (MTPA).

To get a fair comparison, 12/8 motor, 12/10 motor and 12/14 motor are designed and optimized with the same stator outer diameter, the same stack length, the same slot fill factor and the same permanent magnet usage. The optimization range for other parameters of the motors are demonstrated in TABLE 1. The motors are operated at the same load and optimized with genetic algorithm (GA) to achieve the highest efficiency at the rated point. As shown in Figure 1, the efficiency of 12/10 motor is the highest and 12/14 motor is the lowest at the rated load after optimization.

TABLE 1. Parameters optimization range of three motors.

Parameter	12/8	12/10	12/14	Unit
Stator inner diameter	[140,150]	[144,154]	[147,160]	mm
Tooth height	[25,30]	[25,30]	[25,30]	mm
Tooth body width	[20,25]	[20,25]	[20,25]	mm
number of conductors per slot	[14,17]	[14,17]	[14,17]	/
angle between V-type PMs	[90,125]	[90,120]	[90,110]	deg
length between two adjacent V-type PMs	[4,10]	[2,8]	[1,6]	mm

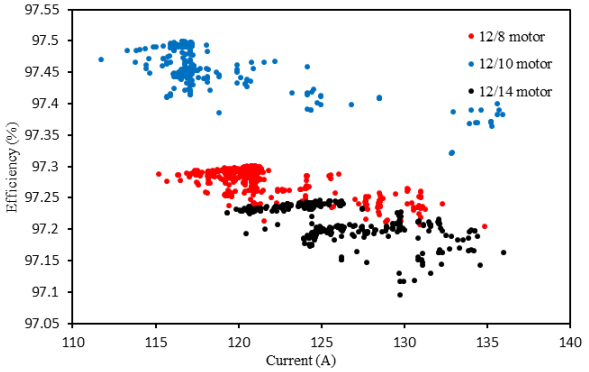

FIGURE 1. The optimization results of the three motors (efficiency vs current).

The final design and the main parameters are listed in Table 2.

III. ELECTROMAGNETIC PERFORMANCES

A. WINDING FACTOR

For FSCW motors, the typical characteristic is the rich harmonic component, which has great impact on various electromagnetic performances of the motor. Besides, the torque capacity of the motor is directly related to the fundamental winding factor. The winding factor of the motor with different pole slot combinations and double layer winding is expressed as:

$$K_{wv} = \sin(\frac{v^*P}{Z}\pi)^* \frac{\sin(v^*P^*\alpha)}{N^* \sin(\frac{v^*P^*\alpha}{N})} \quad (1)$$

TABLE 2. Main parameters of three motors.

Parameter	12/8	12/10	12/14	Unit
Design parameters				
Rated speed		2700		rpm
Rated power		34		kW
Peak power		80		kW
Maximum speed		12000		rpm
Design specifications				
Stator outer diameter		230		mm
Stator inner diameter	144.9	146.5	151.3	mm
Air-gap length		0.6		mm
Magnet mass		1.29		kg
Shaft radius		64		mm
Active length		88		mm
Slot opening		2		mm
Slot fill factor		50		%
Tooth height	28.4	27.8	26.2	mm
Tooth body width	23.7	23.5	23.0	mm
Magnet material		N48UH		

where P is the pole pair number of the motor, $v = k/P$, $k \in N^+$ is the harmonic order, Z is the slot number, $N = Z/r$ and r is the maximum common divisor of the slot number and the multiple of the pole number and phase number, α is the electric angle between the adjacent slots.

From (1), it can be found out that the winding factor of FSCW motor has periodicity and symmetry, which is the main cause of the low order harmonics for FSCW motors and its irreducibility. The three-phase magnetomotive force (MMF) of the motor can be derived from the winding factor, as shown in (2) and the calculation results for the three motors are displayed in Figure 2.

$$K_v = \begin{cases} \dfrac{K_{wv}}{v} & \text{v} \neq (3^*\text{j})/\text{P} \\ 0 & \text{v} = (3^*\text{j})/\text{P} \end{cases} \quad j \in N^+ \tag{2}$$

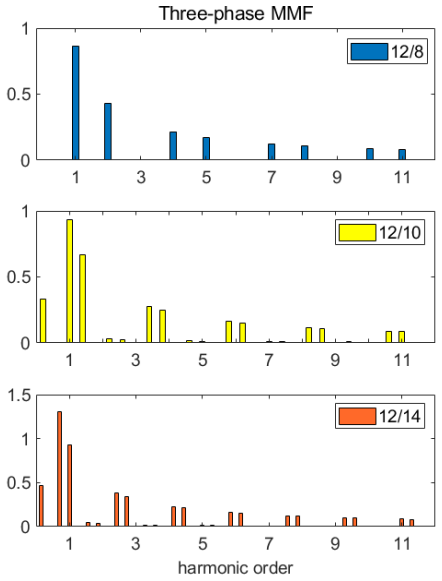

FIGURE 2. Three-phase MMF factor for the three motors.

From Figure 2, all motors have rich harmonic components in low order harmonics. The sub-harmonics of 12/10 motor and 12/14 motor is quite large, which is the main cause of the losses and motor vibration. There is no sub-harmonics for 12/8 motor. The super harmonics amplitude of 12/10 motor is lower than 12/14 motor, except the amplitude at $7/5^{\text{th}}$ order. For 12/8 motor, the super harmonic amplitudes are much lower than the other two. Nevertheless, 12/10 motor and 12/14 motor have high fundamental winding factor, equal 0.933, much higher than that of 12/8 motor, 0.866, which contributes to higher output torque.

B. INDUCTANCES AND SALIENCY

The inductances of the motor are key issues, which are closely related to the power factor and the flux weakening capability for motors. Besides, the ratio of the q-axis inductance over the d-axis inductance, named saliency, contributes to the torque capacity under MTPA control. The d-axis and q-axis inductance of the motor and the saliency are expressed as [11]:

$$L_{ad,aq} = \frac{m}{\pi} D_{equ} L_{ef} N_1^2 \frac{K_{d,q}}{K_{sd,sq}} \lambda_{ad,aq} \sum \left(\frac{K_v}{P}\right)^2 \tag{3}$$

$$L_{d,q} = L_{ad,aq} + L_{\delta d,\delta q} \tag{4}$$

$$saliency = \frac{L_q}{L_d} \tag{5}$$

where m is the phase number, D_{equ} is the equivalent diameter of analytical calculation, L_{ef} is the effective stack length, N_1 is the number of turns per phase in serials, $K_{d,q}$ are armature reaction factors in d- and q-axis, $K_{sd,sq}$ are the saturation factors of the d- and q- axis magnetic circuits, $\lambda_{ad,aq}$ are the specific permeances of the d- and q- axis magnetic circuits, $L_{ad,aq}$ is the armature inductances and $L_{\delta d,\delta q}$ is the leakage inductances.

From (3), it can be found out that the armature inductances of the motor are related to the winding factors of the motors and the pole number. The sum of the harmonic coefficients of the three motors are close. Moreover, the inductances are also influenced by the armature reaction in d- and q-axis, making the saliency of the motor with different pole slot combinations distinguished. Another factor for the inductances is the saturation condition of the motors. As consequence, the inductances and the saliency change with the different operating current.

The d-axis armature inductances of 12/14 motor is the highest for its largest equivalent diameter. Besides, the leakage inductances of 12/14 motor is the largest and that of 12/8 motor is the smallest, as can be judged from [11]. Therefore, 12/8 motor has the smallest d-axis inductance while 12/14 motor has the largest d-axis inductance, as can be seen from Figure 3.

The q-axis inductance is greatly influenced by the permeance of the q-axis magnetic circuits, which is closely related to the q-axis flux path of the motors and differentiates with the motors with different pole slot combinations.

The q-axis flux distribution of the three IPMSMs are demonstrated in Figure 4. Compared to 12/8 motor, the

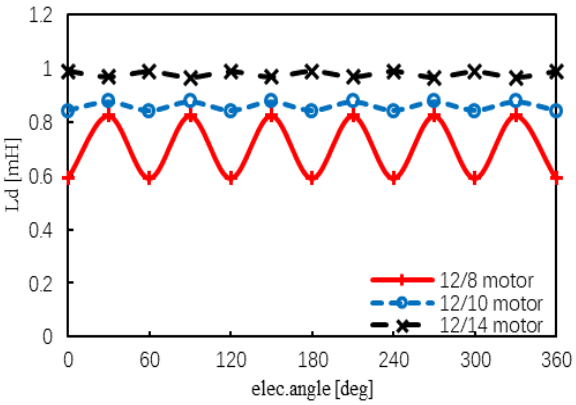

FIGURE 3. d-axis inductances of the three motors at no-load.

q-axis flux of 12/10 motor and 12/14 motor crosses the magnetic bridge between the V-type permanent magnet, which is highly saturated and the permeance of the q-axis magnetic circuits declines greatly as consequence. Even more q-axis flux of 12/14 motor crosses the saturated magnetic bridge than 12/10 motor, comparing Fig. 3. (b) and (c). Therefore, the saliency of 12/8 motor is the highest and 12/14 motor has the lowest saliency, as shown in Figure 5.

The saturation effect dominated with high current, which indicated the permeance of the q-axis magnetic circuits is declined for all motors. However, the descending trend of the saliency for 12/10 motor and 12/14 motor is not obvious as the saturation factors of the d- and q- axis magnetic circuits are close. To be mentioned, the saliency of 12/14 motor is close to one. The advantage of the FSCW IPMSM for 12/14 motor is lost.

C. POWER FACTOR AND TORQUE CAPACITY

Based upon the inductances and saliency from the FEA analysis, the power factor is further analyzed and compared. It is complicated to figure out the relationship between the saliency and the power factor since the MTPA control method applied. Therefore, the relationship between the power factor and the inductances are further investigated as shown in Figure 6.

From Figure 6, it should be noted that there exists an optimal saliency for motors to get the highest power factor. However, it is obvious that the power factor is mainly influenced with the d-axis inductance while almost staying unchanged with the saliency. With the higher d-axis inductance, the power factor declines. Therefore, it can be concluded that the power factor of 12/8 motor is higher than the other two owing to the smallest d-axis inductance, which means 12/8 motor can achieve the highest power capacity using the same inverter.

The torque capacity of the motor is also influenced by the inductances and the saliency of the motor. 12/8 motor has the highest saliency but the lowest fundamental winding factor, which imply the largest reluctance torque and

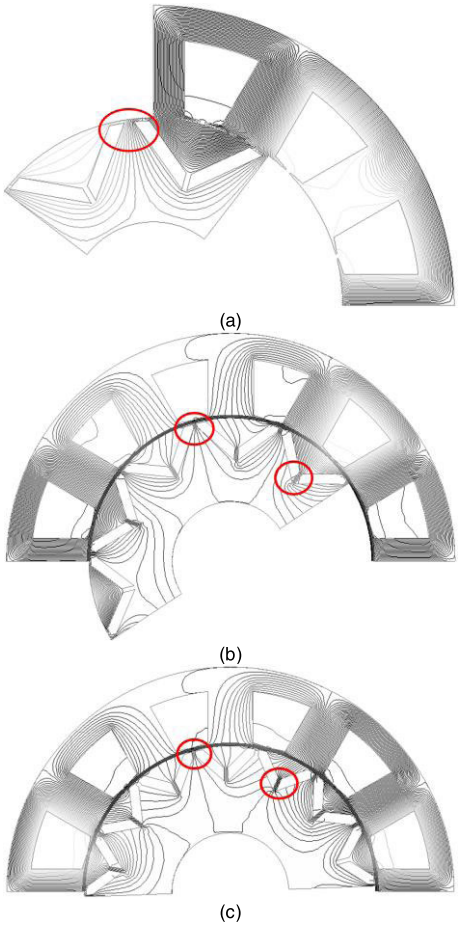

FIGURE 4. Q-axis flux distribution for motors at 100 arms. (a). 12/8 motor. (b). 12/10 motor. (c). 12/14 motor.

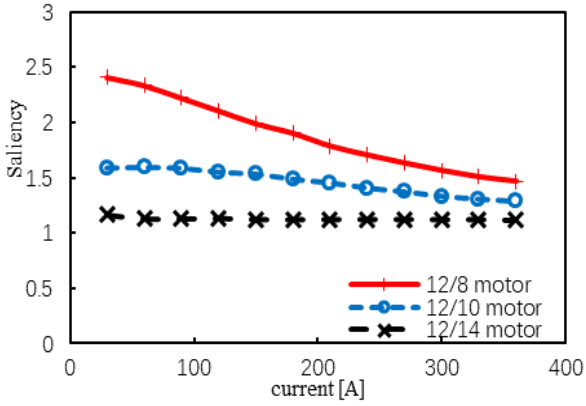

FIGURE 5. Saliency versus current.

the smallest PM torque. It is beneficial for 12/8 motor to gain higher torque with higher saliency under low torque condition. However, there is no superiority when the current is high and the saliency goes down greatly for 12/8 motor. As shown in Figure 7, with the current rising, 12/8 motor gain less torque with the same current. 12/10 motor has a slight advantage over 12/14 motor for the higher saliency.

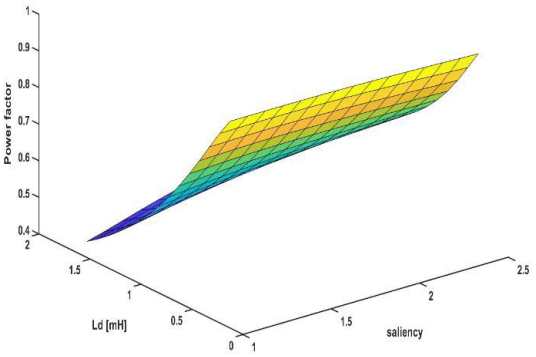

FIGURE 6. Power factor vs inductances with the same current supply.

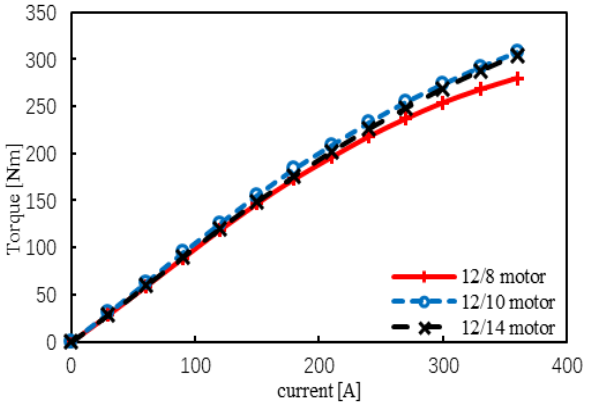

FIGURE 7. Torque characteristic.

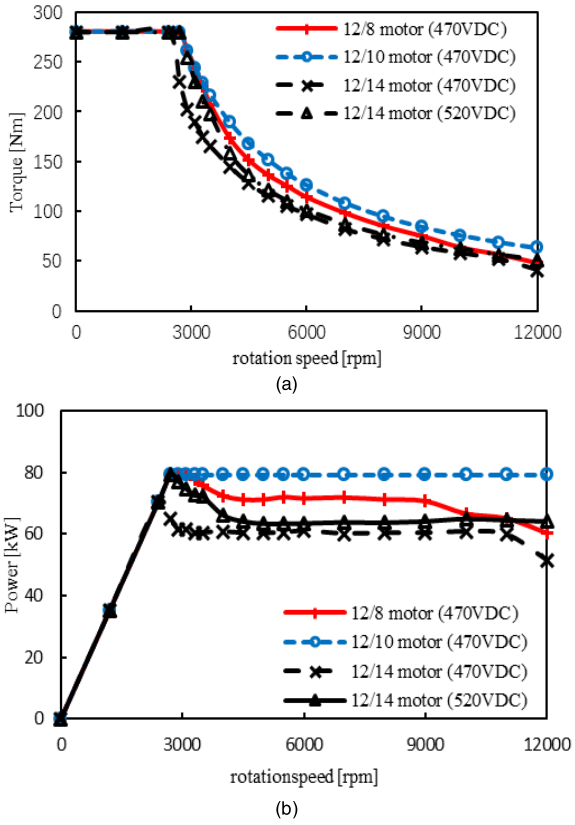

FIGURE 8. Traction curve. (a). Torque vs speed. (b). Power vs speed.

D. CONSTANT POWER SPEED RANGE

The DC link voltage is limited, which largely restricts the power capacity of the motors. For 12/14 motor, the d-axis inductance is too high that the power factor at the peak current is very low, as shown in Table. 3. With the same limited DC link voltage, 12/14 motor is not capable of generating the same power as 12/10 motor and 12/8 motor. As depicted in Figure 8, 12/14 motor can merely reach the peak power of 70 kW when the DC bus voltage is 470 V. The knee point can reach 2700 rpm by increasing the DC bus voltage to 520 V_{DC} for 12/14 motor.

TABLE 3. The CPSR related parameters.

Parameter	12/8	12/10	12/14	Unit
PM flux linkage	0.1133	0.0957	0.0638	Wb
Characteristic current	228	146	91	A
Operating current	360	310	320	A
Voltage distortion @ 80 kW, 2700 rpm	1.46	1.09	1.11	
Power factor @ 80 kW, 2700 rpm	0.58	0.60	0.45	

Moreover, the voltage distortion performance and the inductance of the motors influence the CPSR. The voltage distortion of FSCW IPM is large either Spp is too close to 1/3 or too far away [12]. The lower the voltage distortion is, the wider the CPSR will be. A wide CPSR can be obtained when the d-axis inductance is at an optimal value, making the characteristic current equal to the operating current [20]. The CPSR related parameters are listed in Table 2. The characteristic current and the voltage distortion are expressed as:

$$I_{ch} = \frac{\Psi_{PM}}{L_d} \tag{6}$$

$$VD = \frac{U_{\max}}{\sqrt{2}U_{rms}} \tag{7}$$

where I_{ch} is the characteristic current and ΨPM is the PM flux linkage, U_{max} is the maximum value of the line-line voltage and U_{rms} is the valid values of the line-line voltage.

The CPSR of the three motors are quite different, as shown in Figure 8. Comparing the three motors, 12/10 motor has wide CPSR owing to small voltage distortion and small gap between the characteristic current and the operating current. For 12/8 motor and 12/14 motor, the huge voltage distortion or the large gap between the characteristic current and the operating current narrows the CPSR. Therefore, 12/14 motor is the worst choice owing to both the smallest power capacity and the narrow CPSR.

E. EFFICIENCY AND LOSSES

The losses include the iron loss, the PM eddy current loss, the copper loss and the mechanical loss. The efficiency can be expressed as (8), as shown at the bottom of the next page,

where I is the current, n is the rotation speed, T is the torque, p_{iron} is the iron loss, p_{PM} is the PM eddy current loss, p_{cu} is the copper loss, including alternating current (AC) copper loss and direct current (DC) copper loss, and p_{mec} is the mechanical loss.

For the three motors, the winding DC resistance of the three motors are close. Hence, only current is considered in terms of DC copper loss. Besides, the mechanical loss is defined as the same due to the same motor dimension. As can be referred from (8), the efficiency is influenced by the current and the rotation speed simultaneously. Therefore, Iron loss, PM eddy current loss, and AC copper loss of the three motors are simulated and analyzed to investigate the efficiency map.

1) THE EFFICIENCY EVALUATION AT CONSTANT TORQUE AREA

In the constant-torque area, the motor is under MTPA control, meaning the same torque with the identical current. Iron loss, PM eddy current loss, and AC copper loss grow monotonously with the rotation speed. To simplify the analysis, iron loss, AC copper loss, and PM eddy current loss are simulated and compared with the various current at the specific speed.

The relationship between the iron loss and the current at the rated speed is shown in Figure 9. 12/14 motor is likely to have the highest iron loss for the largest pole number, namely, the highest frequency and 12/8 motor the lowest.

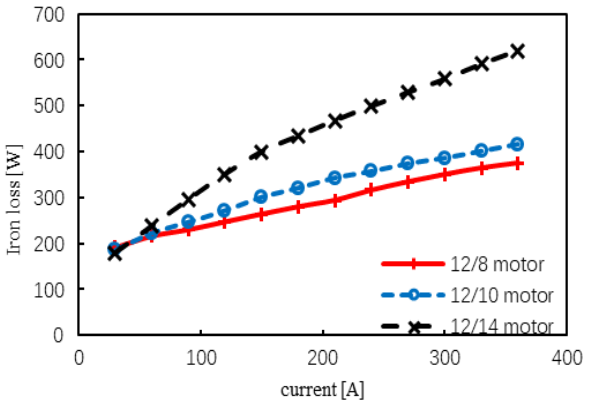

FIGURE 9. Iron loss versus current at the rated speed.

The iron loss is very close for the three motors under low torque condition. For motors with larger pole number, smaller flux linkage per pole contributes to the smaller flux magnetic density in stator yoke, and the smaller stator iron loss as a result. With the current increasing, the motor gets more saturated that the advantage for larger-pole-number motor in stator part wear off. In addition, the increase of the iron loss in the rotor part due to the rich harmonic components caused by the armature reaction for all motors highlight gradually.

The iron loss calculation in the frequency domain is expressed as:

$$p_{iron} = k_h B^2 f + k_c B^2 f^2 + k_e B^{1.5} f^{1.5} \tag{9}$$

where k_h, k_c, k_e are the coefficients of hysteresis, eddy current, and excess losses, B is the magnetic density and f is the frequency.

With formula (9) and the iron loss calculated and simulated in Table 4, it can be found out that 12/10 motor and 12/14 motor have lower normalized iron losses compared to the normalized coefficients of frequency, owing to the lower overall magnetic density distribution than 12/8 motor. Comparing the performances at 360 A and 120 A, higher current leads to the more serious saturation phenomenon and the gap of iron losses between the three motors becomes larger.

TABLE 4. Iron loss results.

Parameter	12/8	12/10	12/14	Unit
Material parameters				
Frequency @2700 rpm	180	225	315	Hz
$K_h f+k_c f^2$	30288	38675	56428	
Normalized ($K_h f+k_c f^2$)	1	1.277	1.863	
Iron losses @ 360 A, 2700 rpm				
Iron loss	374.55	416.09	619.87	W
Normalized iron loss	1	1.11	1.65	
Iron losses @ 120 A, 2700 rpm				
Iron loss	246.61	272.14	351.38	W
Normalized iron loss	1	1.10	1.42	

The PM eddy current loss is related to the PM resistance and the change rate of the flux magnetic density in PM. For motors with higher pole number, the PM resistance will be smaller. However, the harmonic components have bigger influence on the PM eddy current losses, especially when the current is high and the armature reaction is severe. 12/10 motor and 12/14 motor both have the rich harmonic components and thus, the highest PM eddy current losses, especially at the high torque condition. 12/8 motor has only 1/3 PM eddy current loss of 12/10 motor at the peak current, as shown in Figure 10.

The cause of the AC copper loss is similar to the PM eddy current loss. However, the copper size of the motors is identical. Therefore, AC copper loss of 12/14 motor is the highest owing to the richest harmonic components, as shown in Figure 11.

$$\eta = \frac{T(\overrightarrow{I}, n)^* \frac{2\pi n}{60}}{T(\overrightarrow{I}, n)^* \frac{2\pi n}{60} + p_{iron}(\overrightarrow{I}, n) + p_{PM}(\overrightarrow{I}, n) + p_{\mathrm{cu}}(\overrightarrow{I}, n) + P_{mec}(n)} \tag{8}$$

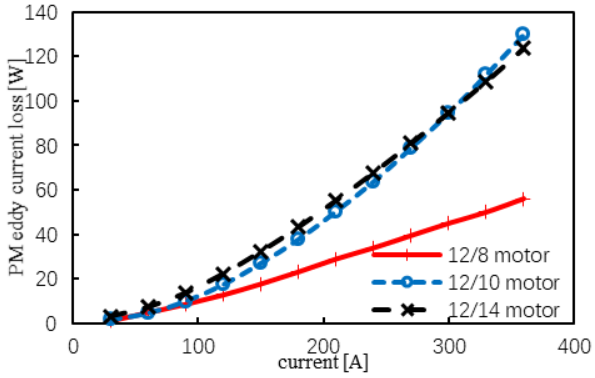

FIGURE 10. PM eddy current loss versus current at the rated speed.

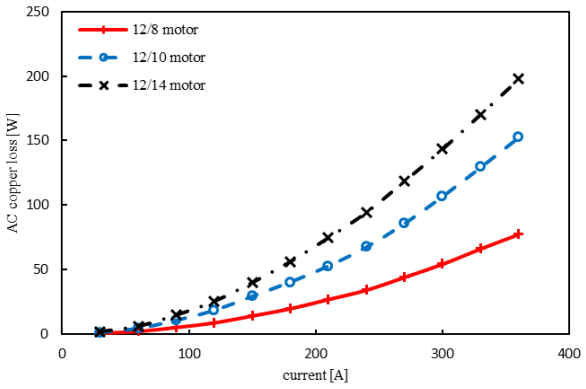

FIGURE 11. AC copper loss versus current at the rated speed.

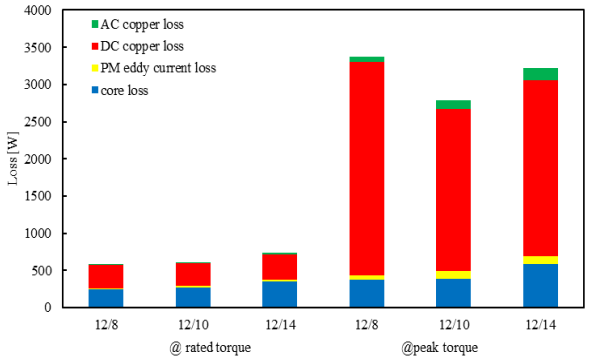

FIGURE 12. Losses @ rated torque and peak torque.

The total losses at the rated torque and peak torque of the three motor are pictured in Figure 12. At the rated torque, 12/14 motor has the highest iron loss and total losses, indicting the lowest efficiency. 12/8 motor requires the highest current to gain the same torque. Thus, the efficiency of 12/8 motor is lower than 12/10 motor and 12/14 motor at the peak torque.

12/10 motor has highest efficiency than the other two over the whole torque range at the rated speed as shown in Figure 13.

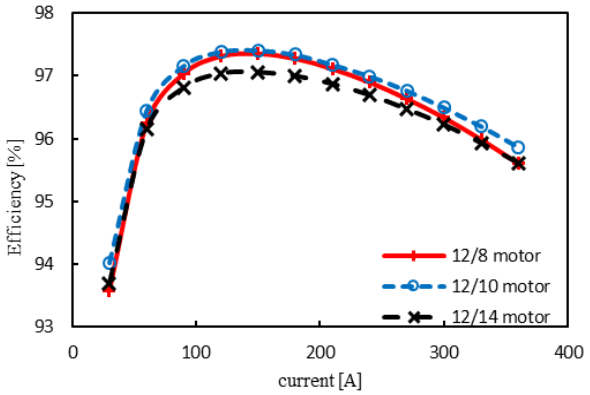

FIGURE 13. Efficiency versus current at the rated speed.

2) THE EFFICIENCY EVALUATION AT FLUX-WEAKENING AREA

For FSCW IPMSM, the voltage distortion is much more severe than the ISDW IPMSM, which might sacrifice the advantages of the wide flux-weakening area.

To increase the speed, higher d-axis current is applied to meet the voltage limitation of the inverter. The variable satisfies the equations below:

$$\begin{cases} U(i_d + ji_q) \approx VD * \sqrt{(\omega\Psi_f + \omega L_d i_d)^2 + (\omega L_q i_q)^2} \\ \qquad\qquad \leq \dfrac{\mathrm{V_{DC}}}{\sqrt{2}} \\ i_d^2 + i_q^2 \leq I_{\mathrm{lim}}^2 \end{cases} \tag{10}$$

where U is the induced line-line voltage, VD is the voltage distortion of the induced voltage, w is the angular velocity, $w = 2\pi\ pn/60$, Ψ_f is the main flux linkage, i_d is the d-axis current and i_q is the q-axis current, V_{DC} is the DC bus voltage of the inverter and I_{lim} is the maximum current of the inverter.

D-axis current close to the characteristic current and lower q-axis current are preferred to get lower induced voltage, as can be induced from (10). Besides, the current has direct impact on the voltage distortion, which further influence the induced voltage. To figure out this, the voltage distortion and the induced line-line voltage varied with the current under different power angle of 12/8 motor are demonstrated in Figure 14.

As shown in Figure 14. (a), there exists an optimal combination of current to meet the lowest induced voltage. The larger the power angle is, the higher the optimal current is. The voltage distortion reaches the lowest value with a specific current value for 12/8 motor, around160 A, especially when the power angle is large, as depicted in Figure 14. (b).

For FSCW IPMSMs, the peak operating current is higher than the characteristic current. As shown in Figure 15, the current of 12/8 motor declined continually without considering the voltage distortion and the voltage constrain. Comparatively, the current of 12/8 motor decreases sharply and gradually becomes constant, close to the optimal current, owing to the voltage distortion and the limited DC bus voltage.

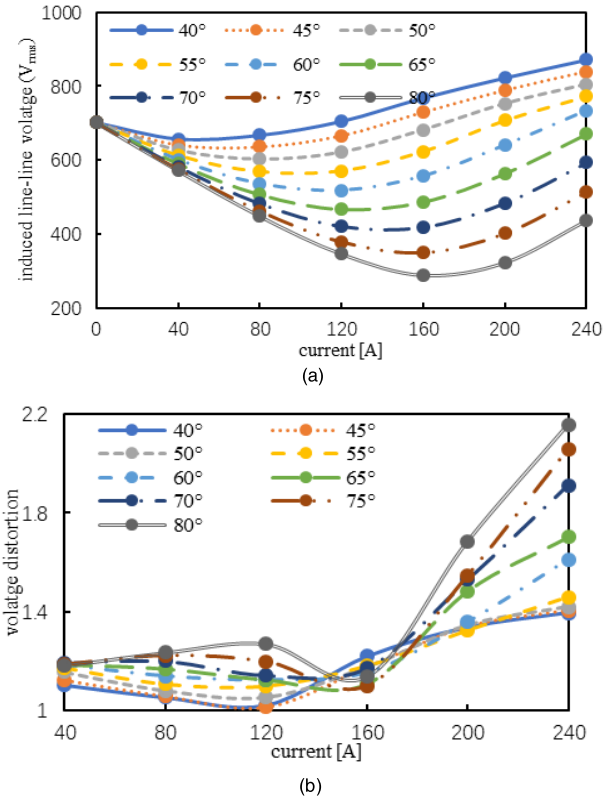

FIGURE 14. (a). induced line-line voltage varied with the current. (b). voltage distortion varied with the current. (12/8 motor).

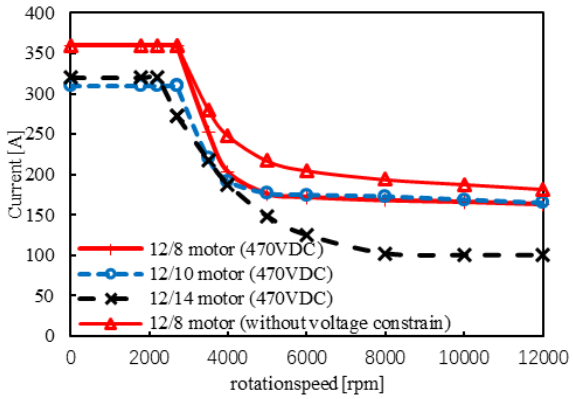

FIGURE 15. Traction curve (current vs speed).

Much higher iron loss and PM eddy current loss can be produced in the flux-weakening area due to the high speed. The iron loss and the PM eddy current loss versus power angle at the maximum speed at 200Arms are pictured in Figure 16-17.

With the larger power angle, the iron loss is reduced owing to the weakened flux linkage. It is noted that 12/8 motor has lower iron loss than 12/10 motor when the power angle is over 55°.

Results are rather different with the PM eddy current loss. The PM eddy current loss is magnificent at high speed. It should be noted that, 12/10 motor and 12/14 motor have

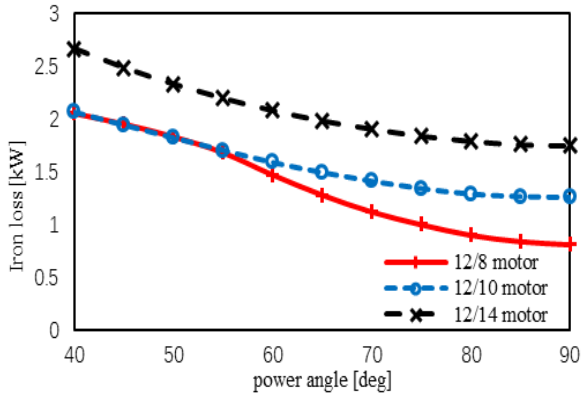

FIGURE 16. Iron loss versus phase angle at the maximum speed at 200A_{rms}.

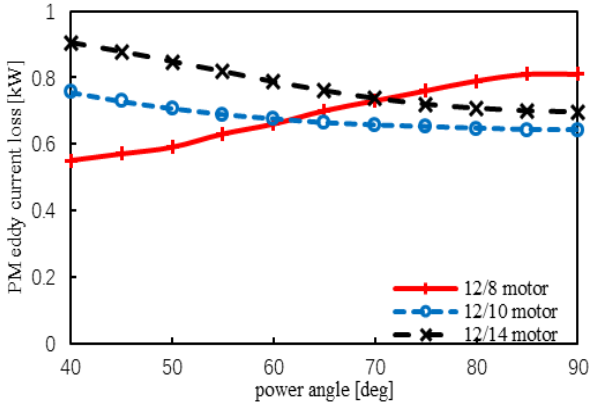

FIGURE 17. PM eddy current loss versus phase angle at the maximum speed at 200A_{rms}.

lower PM eddy current loss with higher power angle. On the opposite, 12/8 motor has higher PM eddy current loss with the power angle increasing. The difference lies in the different effect of the q-axis current on the PM eddy current loss of 12/8 motor, 12/10 motor and 12/14 motor. As demonstrated in Figure 5, less q-axis flux has chance to get through the PM for 12/8 motor. Thus, the PM eddy current loss increased by the q-axis current is also much smaller. With the increase of the power angle, the q-axis current reduced greatly and the PM eddy current loss of 12/10 motor and 12/14 motor decrease as a result. On the contrary, the PM eddy current loss caused by the increase of d-axis current for 12/8 motor is over the decrease of the q-axis current.

3) THE EFFICIENCY MAP

The efficiency map of the three motors are further calculated with Ansys Maxwell. As demonstrated in Figure 18, 12/10 motor has the largest high-efficiency area (efficiency higher than 95%). However, the efficiency of the three motors in the high-speed region has little difference. The mechanical loss increases sharply with the speed and occupies a large proportion in the high-speed range while the total losses, including the iron loss, PM eddy current loss, and copper loss is close.

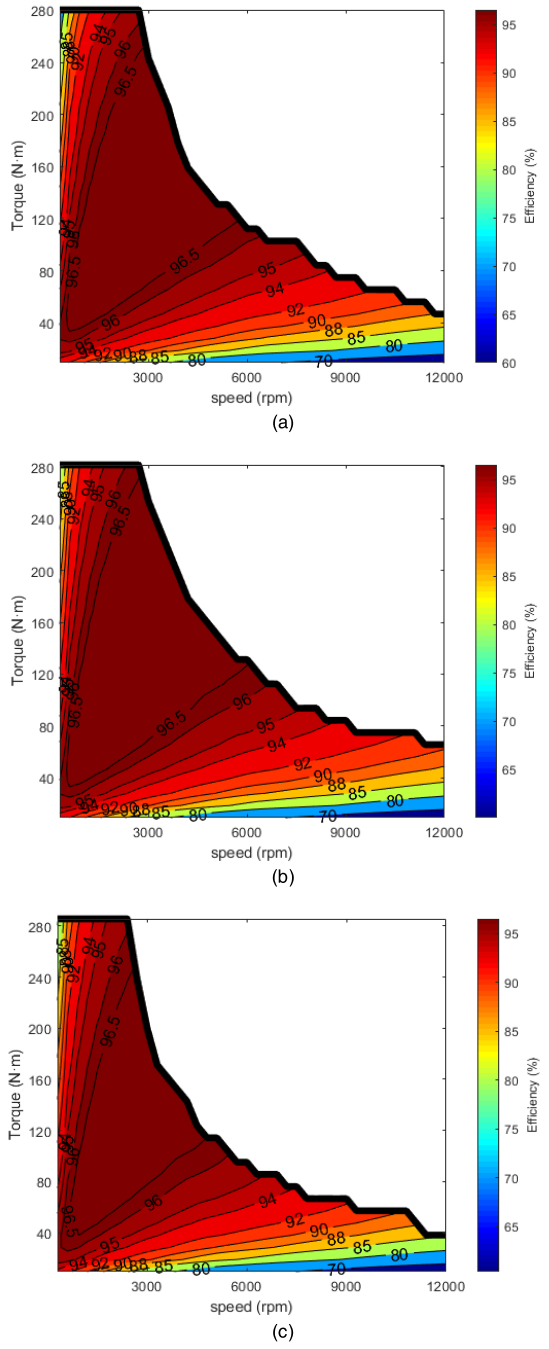

FIGURE 18. The efficiency map. (a). 12/8 motor. (b). 12/10 motor. (c). 12/14 motor.

F. DEMAGNETIZATION CAPABILITY

To compare the demagnetization capability of the motors, the demagnetization ratio is calculated and expressed as:

$$ratio = 1 - \frac{E_{0-ad}}{E_{0-bd}} \tag{11}$$

where E_{0-ad} is the no-load back electromotive force (EMF) after demagnetization and E_{0-bd} is the no-load back EMF before demagnetization.

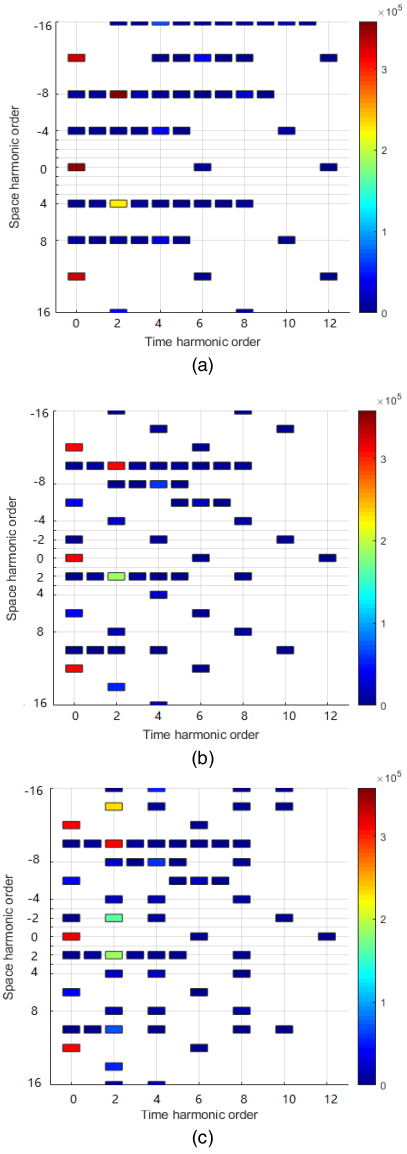

FIGURE 19. Radial force density spectrum at 120 Nm 2700 rpm. (a). 12/8 motor. (b). 12/10 motor. (c). 12/14 motor.

The demagnetization capability is influenced by the harmonic components of the motors. With richer harmonic components, motors are easier to get demagnetized. The simulation is carried out at 160 °C with the maximum d-axis current, 400 A, allowed by the inverter. As shown in Table 5, at worst case scenario,12/14 motor has the largest demagnetization ratio due to the richest harmonic components. From the perspective of the demagnetization capability, 12/8 motor is the best choice. However, the demagnetization capability is rather weak for all the three motors.

IV. OTHER PERFORMANCES

The vibration of the motor is related with the space harmonic components of the radial force density and the time frequency compared to the natural frequency of the motor. The radial

TABLE 5. Demagnetization resistance of the motors.

Parameter	12/8	12/10	12/14	Unit
No-load back EMF (before demagnetization)	144	149	137	V_{rms}
No-load back EMF (after demagnetization)	36	24	18	V_{rms}
demagnetization ratio	75.0	83.9	86.9	%

TABLE 6. Vibration of the motors.

Parameter	12/8	12/10	12/14	Unit
Maximum deformation	0.652	6.281	4.77	μm
Maximum velocity	0.027	6.255	18.7	μm/s

force density spectrum at 120 Nm 2700 rpm of the three motors is displayed in Figure 19.

The spectrum of the radial force density is expressed as (m, nf_e), in which m is the space harmonic order and n is the time harmonic order. The main harmonic components (except the space harmonic order equals zero) is $(4, 2f_e)$, $(2, 2f_e)$ and $(\pm 2, 2f_e)$ for 12/8 motor, 12/10 motor, and 12/14 motor, respectively. The vibration is inversely proportional to the fourth power of the space harmonic order of the radial force density. Therefore, the 12/14 motor has the worst vibration performance, as shown in Table 5.

As shown in Table 5, 12/14 motor has the maximum velocity and the severest vibration performance. On the contrary, 12/8 motor has the minimum deformation with 6.52e-7 m at the rated point. The vibration results are in consistent with the radial force density spectrum of the motors.

V. CONCLUSION

This paper designed three FSCW IPMSMs with 12 slots and presented comprehensive comparison of the motor performances.

The selection principle for FSCW IPMSMs with the same slot is investigated in the paper based on the analysis of the stator winding factor. Furthermore, the harmonic components of the motors are the main cause of different motor performances, including the inductances, the losses, the demagnetization capability and the NVH performances.

For FSCW IPMSMs with the same slot, the pole number slightly less than the slot number is preferred to obtain the high torque owing to the high fundamental winding factor and the relatively high saliency. The iron loss, the PM eddy current loss, and the AC copper loss increase with the frequency and the harmonic components. Therefore, the high efficiency can be obtained in high-load and low-speed region for motors with the pole number slightly less than the slot number due to low copper loss at the same load. However, the demagnetization capability and the NVH performances of motors with close slot and pole number are poor, due to the rich harmonic components.

12/14 FSCW IPMSM is not suitable for EV motors. For 12/10 FSCW IPMSM, wide high-efficiency area and CPSR can be achieved owing to the high fundamental winding factor and relatively low pole number. 12/8 FSCW IPMSM has great advantages in terms of NVH performances and anti-demagnetization capability due to the small harmonic components.

REFERENCES

[1] Z. Yang, F. Shang, I. P. Brown, and M. Krishnamurthy, "Comparative study of interior permanent magnet, induction, and switched reluctance motor drives for EV and HEV applications," *IEEE Trans. Transport. Electrific.*, vol. 1, no. 3, pp. 245–254, Oct. 2015.

[2] S. Williamson, M. Lukic, and A. Emadi, "Comprehensive drive train efficiency analysis of hybrid electric and fuel cell vehicles based on motor-controller efficiency modeling," *IEEE Trans. Power Electron.*, vol. 21, no. 3, pp. 730–740, May 2006.

[3] T. Finken, M. Felden, and K. Hameyer, "Comparison and design of different electrical machine types regarding their applicability in hybrid electrical vehicles," in *Proc. 18th Int. Conf. Electr. Mach.*, Sep. 2008, pp. 1–5.

[4] A. M. El-Refaie, "Fractional-slot concentrated-windings synchronous permanent magnet machines: Opportunities and challenges," *IEEE Trans. Ind. Electron.*, vol. 57, no. 1, pp. 107–121, Jan. 2010.

[5] P. Cros and J. Viarouge, "Synthesis of high performance PM motors with concentrated windings," *IEEE Trans. Energy Convers.*, vol. 17, no. 2, pp. 248–253, Jun. 2002.

[6] J. Rao, Y. Gao, D. Li, and R. Qu, "Performance analysis of interior permanent magnet motor using overlapping windings with fractional ratio of slot to pole pair," *IEEE Trans. Appl. Supercond.*, vol. 26, no. 7, Oct. 2016, Art. no. 0610005.

[7] G. De Donato, F. G. Capponi, G. A. Rivellini, and F. Caricchi, "Integral-slot versus fractional-slot concentrated-winding axial-flux permanent-magnet machines: Comparative design, FEA, and experimental tests," *IEEE Trans. Ind. Appl.*, vol. 48, no. 5, pp. 1487–1495, Sep. 2012.

[8] L. Xu, G. Liu, W. Zhao, J. Ji, H. Zhou, W. Zhao, and T. Jiang, "Quantitative comparison of integral and fractional slot permanent magnet Vernier motors," *IEEE Trans. Energy Convers.*, vol. 30, no. 4, pp. 1483–1495, Dec. 2015.

[9] P. B. Reddy, A. M. El-Refaie, K.-K. Huh, J. K. Tangudu, and T. M. Jahns, "Comparison of interior and surface PM machines equipped with fractional-slot concentrated windings for hybrid traction applications," *IEEE Trans. Energy Convers.*, vol. 27, no. 3, pp. 593–602, Sep. 2012.

[10] S.-K. Lee, G.-H. Kang, and J. Hur, "Finite element computation of magnetic vibration sources in 100 kW two fractional-slot interior permanent magnet machines for ship," *IEEE Trans. Magn.*, vol. 48, no. 2, pp. 867–870, Feb. 2012.

[11] R. Ni, G. Wang, X. Gui, and D. Xu, "Investigation of d- and q-axis inductances influenced by slot-pole combinations based on axial flux permanent-magnet machines," *IEEE Trans. Ind. Electron.*, vol. 61, no. 9, pp. 4539–4551, Sep. 2014.

[12] Z. Q. Zhu, D. Wu, and X. Ge, "Investigation of voltage distortion in fractional slot interior permanent magnet machines having different slot and pole number combinations," *IEEE Trans. Energy Convers.*, vol. 31, no. 3, pp. 1192–1201, Sep. 2016.

[13] D. Wu and Z. Q. Zhu, "On-load voltage distortion in fractional slot surface-mounted permanent magnet machines considering local magnetic saturation," *IEEE Trans. Magn.*, vol. 51, no. 8, Aug. 2015, Art. no. 8106410.

[14] Z. Q. Zhu and D. Wu, "On-load voltage distortion in fractional-slot interior permanent magnet machines," *IEEE Trans. Magn.*, vol. 51, no. 10, Oct. 2015, Art. no. 8107809.

[15] S. G. Min and B. Sarlioglu, "Analysis and comparative study of flux weakening capability in fractional-slot concentrated windings," *IEEE Trans. Energy Convers.*, vol. 33, no. 3, pp. 1025–1035, Sep. 2018.

[16] Z. Zhu, Y. Huang, J. Dong, and F. Peng, "Investigation study of the influence of pole numbers on torque density and flux-weakening ability of fractional slot concentrated winding wheel-hub machines," *IEEE Access*, vol. 7, pp. 84918–84928, 2019.

[17] Y. Liu, Z. Zhu, C. Gan, S. Brockway, and C. Hilton, "Comparison of optimal slot/pole number combinations in fractional slot permanent magnet synchronous machines having similar slot and pole numbers," *J. Eng.*, vol. 2019, no. 17, pp. 4585–4589, Jun. 2019.
[18] E. Fornasiero, L. Alberti, N. Bianchi, and S. Bolognani, "Considerations on selecting fractional-slot nonoverlapped coil windings," *IEEE Trans. Ind. Appl.*, vol. 49, no. 3, pp. 1316–1324, May 2013.
[19] E. Carraro, N. Bianchi, S. Zhang, and M. Koch, "Design and performance comparison of fractional slot concentrated winding spoke type synchronous motors with different slot-pole combinations," *IEEE Trans. Ind. Appl.*, vol. 54, no. 3, pp. 2276–2284, May 2018.
[20] C. Zhou, X. Huang, Y. Fang, and L. Wu, "Comparison of PMSMs with different rotor structures for EV application," in *Proc. 13th Int. Conf. Electr. Mach. (ICEM)*, Alexandroupoli, Greece, Sep. 2018, pp. 609–614.

CHENXI ZHOU was born in Zhejiang, China, in 1994. She received the B.S. degree in electrical engineering and its automation from Zhejiang University, Hangzhou, China, in 2016, where she is currently pursuing the Ph.D. degree in electrical engineering. Her research interests include the design and optimization of the PMSM applied in electric vehicles.

XIAOYAN HUANG (Member, IEEE) received the B.E. degree in control measurement techniques and instrumentation from Zhejiang University, Hangzhou, China, in 2003, and the Ph.D. degree in electrical machines and drives from the University of Nottingham, Nottingham, U.K., in 2008.

From 2008 to 2009, she was a Research Fellow with the University of Nottingham. She is currently a Professor with the College of Electrical Engineering, Zhejiang University, where she is also working on electrical machines and drives. Her research interests include PM machines and drives for aerospace and traction applications, and generator system for urban networks.

ZHAOKAI LI was born in Lishui, China, in 1993. He received the B.S. and Ph.D. degrees in electrical engineering from Zhejiang University, Hangzhou, China, in 2015 and 2020, respectively.

He is currently a Postdoctoral Researcher with Zhejiang University. His research interests include the analytical modeling of PMSM and the model predictive control. His research interests also include the analytical modeling of PMSM and iron loss analysis.

WENPING CAO (Senior Member, IEEE) received the B.Eng. degree in electrical engineering from Beijing Jiaotong University, Beijing, China, in 1991, and the Ph.D. degree in electrical machines and drives from the University of Nottingham, Nottingham, U.K., in 2004.

He is currently a Chair Professor of Electrical Power Engineering and the Head of the Power Electronics, Machines, and Power System Group, Aston University, Birmingham, U.K. He received the Royal Society Wolfson Research Merit Award, U.K., the Innovator of the Year Award from Newcastle University, U.K., in 2013, the Best Paper Award from the 2013 International Symposium on Linear Drives for Industry Applications, and the Dragon's Den Competition Award from Queen's University Belfast, U.K., in 2014. He was a Semifinalist with the Annual MIT-CHIEF Business Plan Contest, USA, in 2015. He is also the Chairman of the Industrial Electronics Society, the IEEE U.K., and the Ireland Sections. He also serves as an Editor for the IEEE TRANSACTIONS ON POWER ELECTRONICS, the IEEE TRANSACTIONS ON INDUSTRY APPLICATIONS, *IEEE Industry Applications Magazine*, the *IET Power Electronics*, and the *Electric Power Components and Systems*. He is also a chief editor for five special issues and four books.